Design and optimization of bioinspired auxetic structure for biomedical applications

Masoud Shirzad [a], Mahdi Bodaghi [b], Dageon Oh[c], Myunggi Yi[a,c], Seung Yun Nam[a,c,*]

[a] *Industry 4.0 Convergence Bionics Engineering, Pukyong National University, Busan 48513, Korea*

[b] *Department of Engineering, School of Science and Technology, Nottingham Trent University, Nottingham, NG11 8NS, UK*

[c] *Major of Biomedical Engineering, Division of Smart Healthcare, Pukyong National University, Busan 48513, Korea*

Email addresses: synam@pknu.ac.kr

Abstract

Auxetic metastructures are characterized by their unconventional deformation behavior and negative Poisson's ratio (NPR), resulting in lateral expansion under tensile loads rather than normal contraction. They have attracted considerable attention for biomedical applications due to their high energy absorption and biofunctional benefits. Consequently, the present study aims to design and investigate a bioinspired auxetic structure that mimics human organ tissues, such as bone and tendon. The mechanical properties of the scaffolds were experimentally tested using a universal testing machine and verified using the finite element method (FEM) for both conventional auxetic and novel triangle auxetic structures. Furthermore, various gradient triangle auxetic structures are developed and analyzed using FEM to optimize their mechanical and physical properties. The results show that triangle auxetic structures increased Young's modulus and yield strength by 28% and 27.5%, respectively, under compression load and by 35% and 40%, respectively, under tensile load. Moreover, by optimizing the gradient architecture while maintaining a similar porosity, these mechanical properties were further enhanced for both loading conditions.

Keywords: Metastructures, Auxetic biomaterials, Tissue scaffolds, Finite element modeling

1. Introduction

To achieve outstanding mechanical behaviors, proposing unique structures is essential. Metastructures have emerged as a way to fabricate distinctive architected materials with unique properties, including negative and zero Poisson's ratios (NPR and ZPR) (Wang et al., 2022a). Auxetic metastructures, a specific type of metastructure with a negative Poisson's ratio, demonstrate a unique property under external load: stretching auxetic metastructures lead to lateral expansion (Lvov et al., 2022). The potential applications of auxetic structures, such as bone implants, running shoes, shape memory foams, and aeronautics have been identified due to their high energy absorption, variable permeability, and fracture toughness (Francisco et al., 2021; Kolken et al., 2022; Lira et al., 2011; Sahariah et al., 2022). Additionally, auxetic structures can be used to improve the mechanical properties and biofunctionality of tissue engineering scaffolds (Kim et al., 2017). Furthermore, the auxetic structure of the tissue-engineered scaffolds can mimic the negative Poisson's ratios found in natural tissue such as cancellous bone and tendon, which exhibit gradient structures (Ghazlan et al., 2020; Guo et al., 2023; Ruhela et al., 2023; Williams and Lewis, 1982; Zhang et al., 2022c).

Although the design of auxetic structures is valuable in various applications, the precise fabrication of complex 3D architectures has been a challenge (Flamourakis et al., 2020; Warner et al., 2017). Rapid prototyping (RP) presents a promising technique for creating 3D interconnected porous scaffolds through the repetitive deposition of material layers (Ahmed, 2019; Kim et al., 2018; Shirzad et al., 2021). Recently, various RP technologies have been introduced, including selective laser sintering (SLS) (Tortorici et al., 2021), stereolithography (SLA) (Kim et al., 2011), digital light processing (DLP) (Shirzad et al., 2020), and fused deposition modeling (FDM) (Alizadeh-Osgouei et al., 2021). Although each RP technique offers advantages, many limitations often restrict the fabrication of scaffolds. For instance, SLS techniques need post-processing, and preparing materials for DLP and SLA techniques is time-consuming and costly. FDM also can be prone to specific challenges, including limited printing resolution and shape fidelity; however, this method can be a reliable strategy for biomedical applications primarily due to its cost-effectiveness,

rapid fabrication, and various options of materials that can be implemented in intricate architectures (Peng et al., 2022; Sankineni and Ravi Kumar, 2022; Solomon et al., 2021).

Based on the advantages of FDM printing, porous scaffolds with complex structures can be fabricated with high accuracy. The manufactured constructs must possess appropriate mechanical properties matched with the target tissue, such as Young's modulus, yield strength, and Poisson's ratio, which are closely related to pore architecture and porosity (Jiao et al., 2022; Soman et al., 2012; Zhang et al., 2022a). While many studies have focused on optimizing Young's modulus and yield strength, few have addressed the tuning of Poisson's ratio, which requires advanced design (Abifarin et al., 2022; Liu et al., 2018; Nuge et al., 2020). Poisson's ratio characterizes the deformations in the transverse direction of a scaffold, making it necessary to consider in determining the elastic deformation with Young's modulus and yield strength (Soman et al., 2012). Accordingly, the choice of design strategy significantly affects the mechanical investigation of scaffolds. Experimental and finite element methods (FEM) are two effective strategies for predicting the mechanical properties of scaffolds. However, experimental methods can be time-consuming and costly, while FEM can predict the mechanical properties and optimize the geometrical parameters of the scaffolds at a low cost within the shortest feasible time (Sala et al., 2022; Yang et al., 2022).

Therefore, the present study aims to explore novel bioinspired auxetic structures to enhance Young's modulus and yield strength, while maintaining high porosity for both tensile and compression loads. To achieve this goal, both conventional and bioinspired auxetic structures were designed and investigated using experimental and FEM methods. The bioinspired auxetic architecture mimicked the microstructures found in bone, which consist of a combination of convex and concave structures, and in tendon tissues, which features a crimp structure. The bioinspired auxetic architecture incorporated a gradient topology to improve the mechanical properties of scaffolds based on the natural human bone and tendon tissues. Various gradient architectures with different auxetic variables were examined to determine the optimum design with high mechanical properties and porosity for this novel bioinspired architecture. All steps of the present study are visualized in Figure 1.

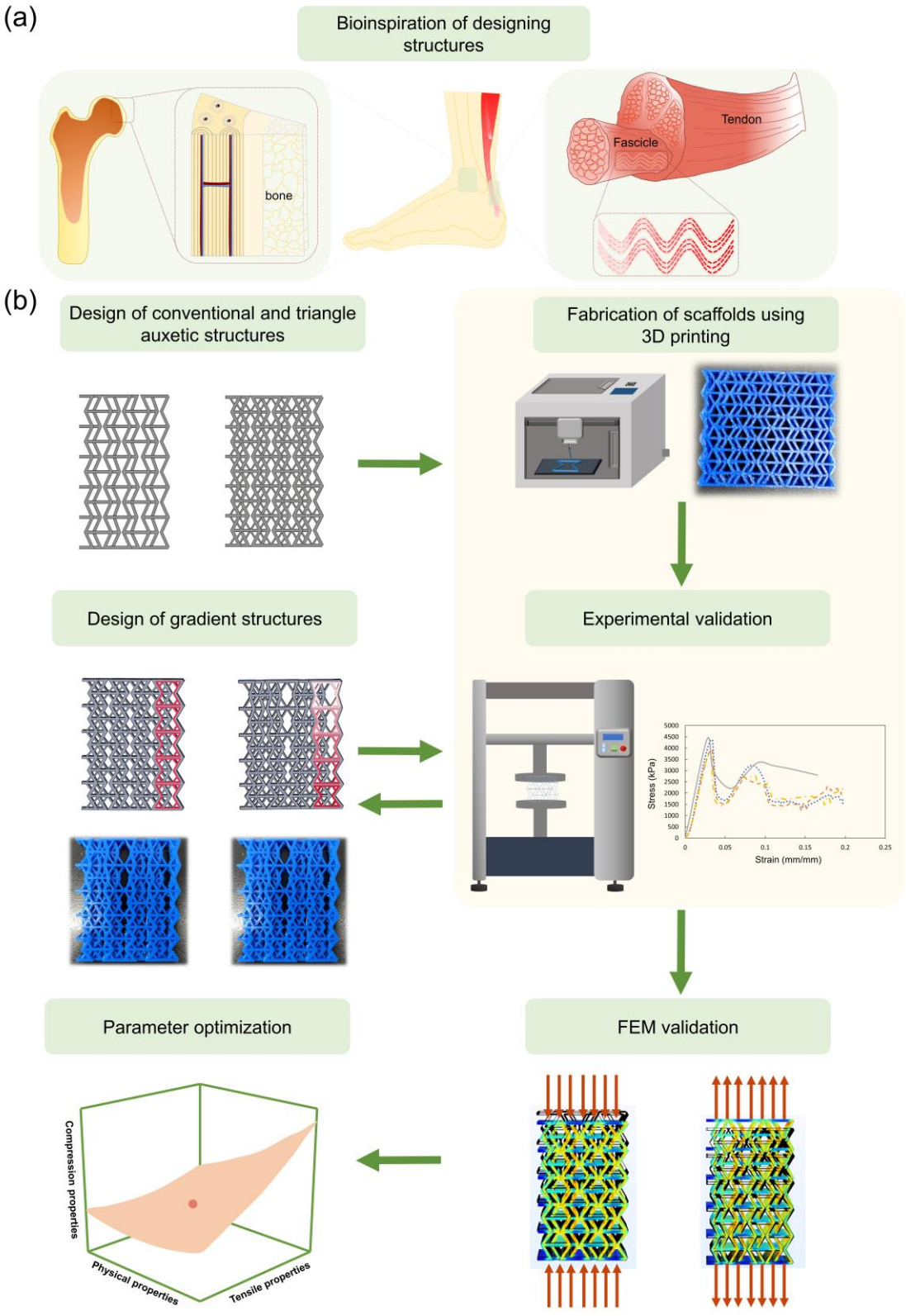

Figure 1. Scheme of auxetic structure development for biomedical applications. (a) Bioinspiration of designing auxetic structures and (b) steps of fabrication, evaluation, and optimization of auxetic scaffolds.

2. Materials and Methods

2.1. Experimental characterization

2.1.1. Design and fabrication of scaffolds

Polylactic acid (PLA) is a biodegradable material with FDA approval for the fabrication of scaffolds (Tanodekaew et al., 2013). In this study, PLA filaments were obtained from Sindoh, and the scaffolds were designed based on the layering of the auxetic substructures. The unit cell dimensions of primary designs are illustrated in Figure 2 and Table 1. Specifically, the concave and convex architectures of the triangle auxetic structure are depicted in orange and green colors in Figure 2b, respectively. To fabricate the scaffolds, the CAD models are converted to stereolithography (.stl) format, and an FDM printer (3D WOX 1, Sindoh) was used to print the designs. To control the size of the unit cells and prevent close pores, even layers were printed with the same size as the unit cell with different architectures. The architecture of each layer and the layering method are illustrated in Figure 3, which were inspired by the structures of the bone and tendon shown in Figure 1.

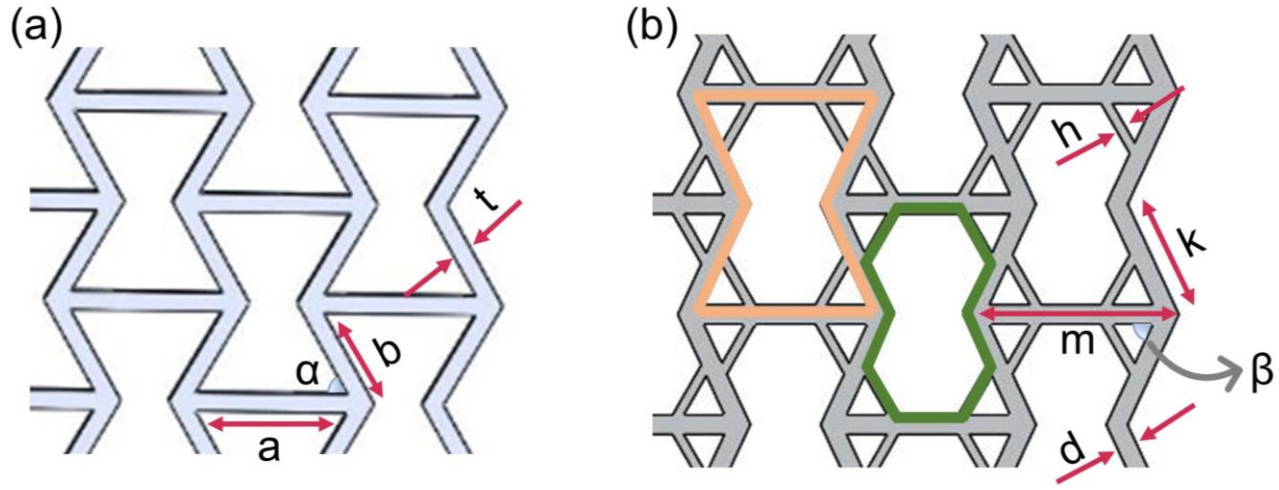

Figure 2. Dimensions of the primary (a) conventional auxetic and (b) triangle auxetic scaffolds

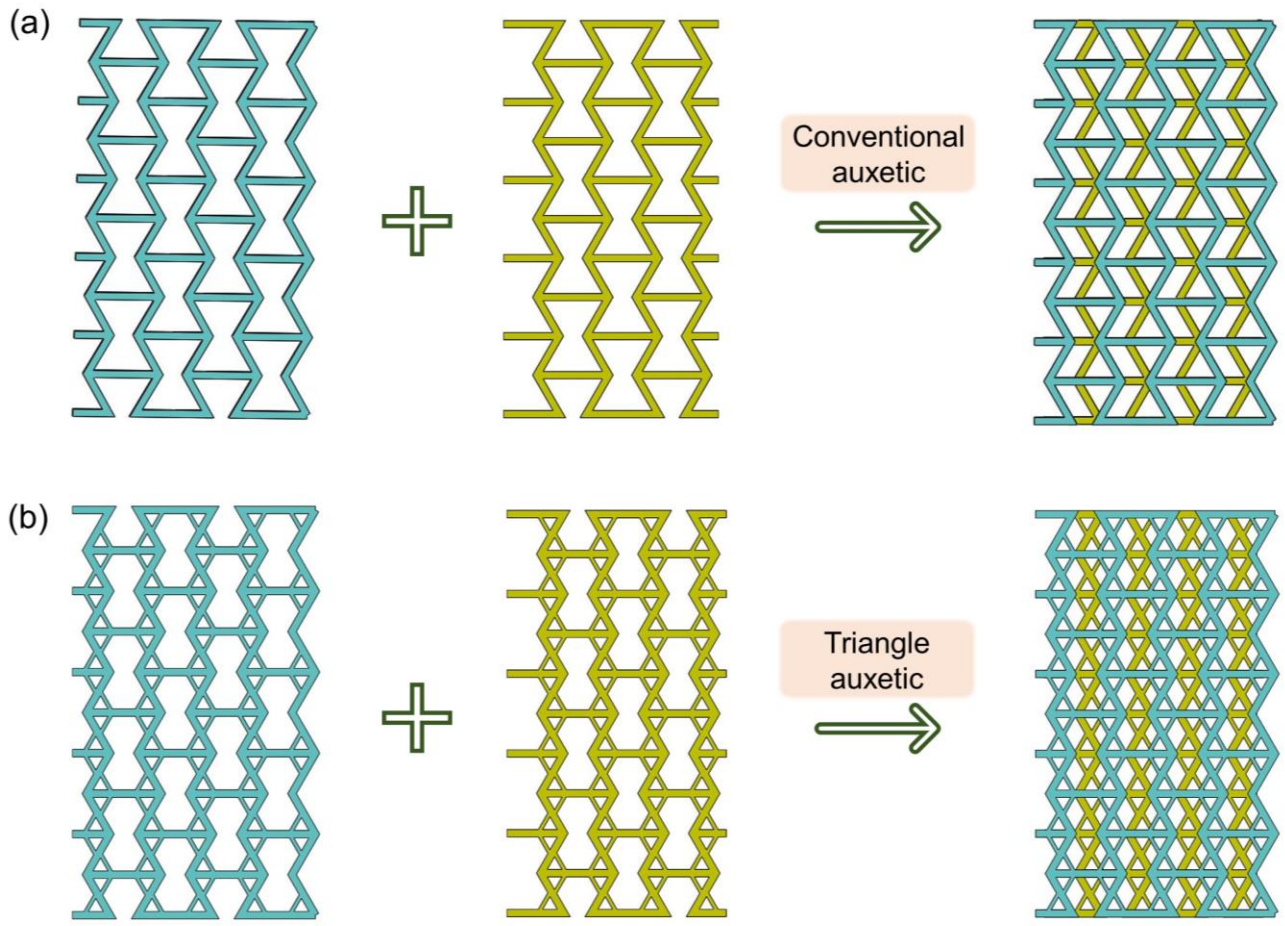

Figure 3. Design and layering of (a) conventional and (b) triangle auxetic structures.

Table 1. Dimensions of the primary design of conventional auxetic and triangle auxetic scaffolds.

Unit cell	Size of components (mm)	Angle (°)	Porosity (%)
Conventional auxetic	a=8 b=5 t=0.8	α=60	74.7
Triangle auxetic	m=8 k=5 d=0.8 h=0.4	β=60	70.2

2.1.2. Experimental mechanical properties

To evaluate the mechanical properties of the scaffolds, compression tests were conducted on bulk and porous architectures using a universal testing machine (LR5K plus, LLOYD Instruments) equipped with a

5 kN load cell. The size of the bulk model is designed according to the ASTM D695 standard for compression test and ASTM D638 for tensile test. The porous scaffolds had dimensions of 26 mm × 13 mm × 47 mm (length, width, and height). The speed of the universal tester head was set at 1 mm/min. To evaluate the mechanical properties of auxetic structures, the load was applied until a 20% reduction in each specimen height was accomplished. Each type of scaffold was tested three times to calculate the average mechanical properties. The stress-strain curve, the most important output of the mechanical test, was plotted based on the apparent stress and non-dimensional strain value. The stress was calculated by dividing the load value on the vertical axis by the initial cross-sectional area of the scaffolds, and the strain values were calculated by dividing the deformation values by the initial scaffolds' height. The 0.2% offset method was used to indicate the yield stress.

Poisson's ratio (υ_{xy}) was calculated using the following formulas as shown in Equation (1-3) (Wang et al., 2022b). The calculation is based on the set of reference points used to compute the average of deformation in various directions. Δ_x and Δ_y present the deformation of two reference points along the x-axis and y-axis, respectively. The strain in the x direction (ε_x) can be calculated by Equation. (1), while the strain in the y direction (ε_y) is defined by Equation. (2). The Poisson's ratio in Equation. (3) is determined by dividing the strain in the x direction by that in the y direction.

$$\varepsilon_x = \frac{\Delta_x}{l_{x0}} \tag{1}$$

$$\varepsilon_y = \frac{\Delta_y}{l_{y0}} \tag{2}$$

$$\upsilon_{xy} = \frac{\varepsilon_x}{\varepsilon_y} \tag{3}$$

where l_{x0} and l_{y0} are the initial distance between the reference points before elongation.

2.2. Finite element models

To evaluate the mechanical properties of the scaffolds, including modulus of elasticity and yield strength, SOLIDWORKS software was used to design the scaffolds, and then they were imported into COMSOL, a

finite element-based software, for mechanical investigation. After importing the CAD models, a 3D structural element (tetrahedral) is used, and the boundary conditions such as loads, strain rate, and displacement are set to match those in the experimental tests. The procedure was repeated for all different topologies. One of the most essential factors of FEM is the relation between element size and the accuracy of the results. Hence, all designs' mesh sensitivity analysis was performed to find the optimum mesh size. This procedure was carried out to show the independency of the results to mesh size. Figure 4 illustrates the schematic method of the mesh sensitivity analysis of the conventional auxetic structure under tensile load.

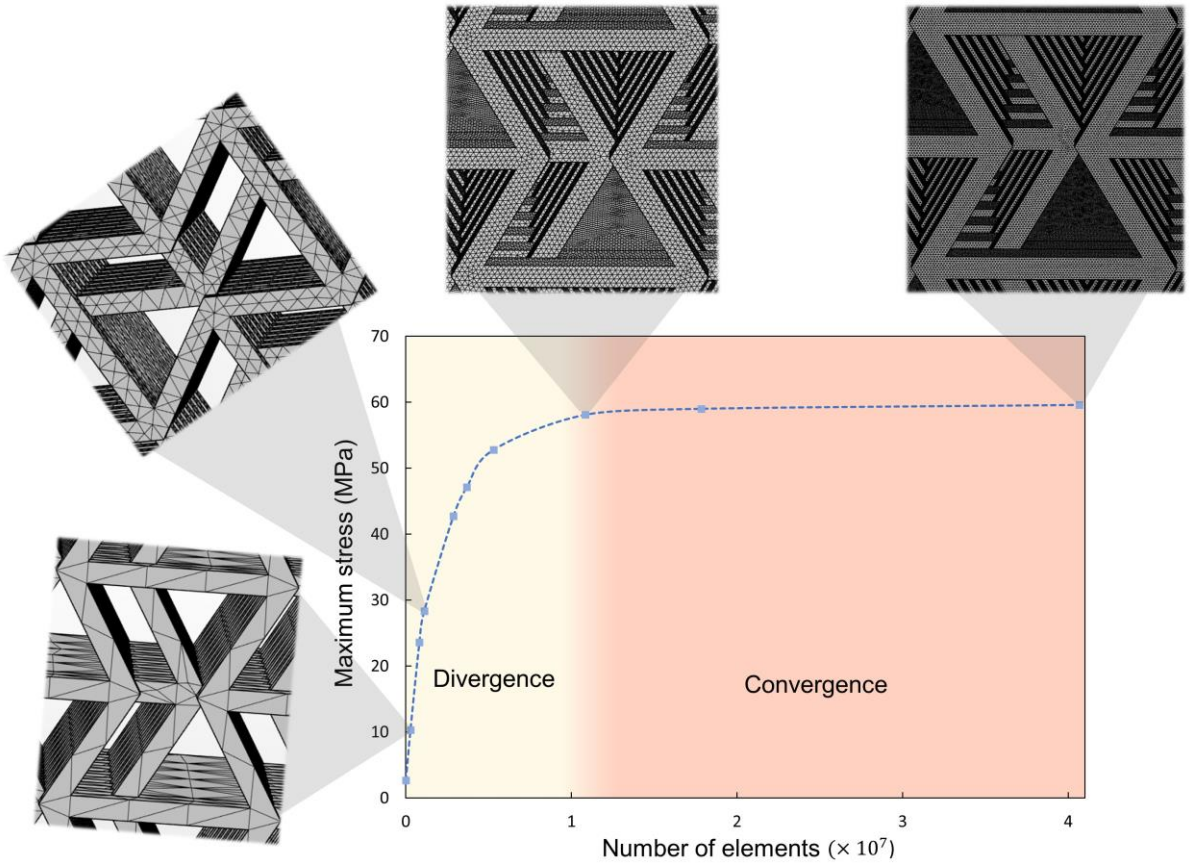

Figure 4. Mesh sensitivity analysis of the conventional auxetic structure for the finite element method.

2.3. Finite element method (FEM)

The FEM software was used to assess the mechanical properties of scaffolds, including elastic modulus, stress concentration, and yield strength. The investigation of mechanical properties was conducted in

sequential steps, starting with the comparison of 3D models of the actual specimens for both the conventional and triangle auxetic structures with their corresponding experimental mechanical properties. After the verification, a gradient triangle auxetic structure with superior mechanical properties was selected for parameter optimization. Figure 1 shows the fabrication, investigation, and optimization procedures for the mechanical properties of the triangle auxetic structures. All the gradient structures of the 3D scaffolds were fabricated with β equal to 55º for the first layer and increasing by 5º for each subsequent layer, resulting in β values of 60º, 65º, 70º, and 75º for the second, third, fourth, and fifth layers, respectively.

3. Results and discussion

3.1. FEM simulation and experimental validation

The CAD-based 3D scaffold models with simple and gradient triangle auxetic structures were fabricated with PLA, as shown in Figure 1. To compare their mechanical properties, a conventional auxetic structure with the same pore size as the triangle auxetic was fabricated using the same material. Additionally, both the conventional and triangle auxetic scaffolds were printed in the same condition. In the first stage, the mechanical properties of the conventional auxetic structure were calculated using experimental and FEM methods. Figures 5 and 6 show the stress-strain curve of the conventional auxetic and triangle auxetic structures. As it is illustrated in Figures 5, 6, 7b, 7d, 8b, and 8d, FEM results are consistent and agree well with the experimental results. However, the FEM results have higher values than the experimental results due to the resolution of the FDM printing, which can induce faults in small struts. These faults locally increase the stress concentration and can result in lower mechanical properties for both conventional and triangle auxetic structures. The results in Figures 5 and 6 were calculated for the a = m = 8 mm, b = k = 5 mm, α = β = 60º, and t = 0.8 mm. The porosity of the conventional auxetic structure is 4.5% higher than the triangle auxetic structure.

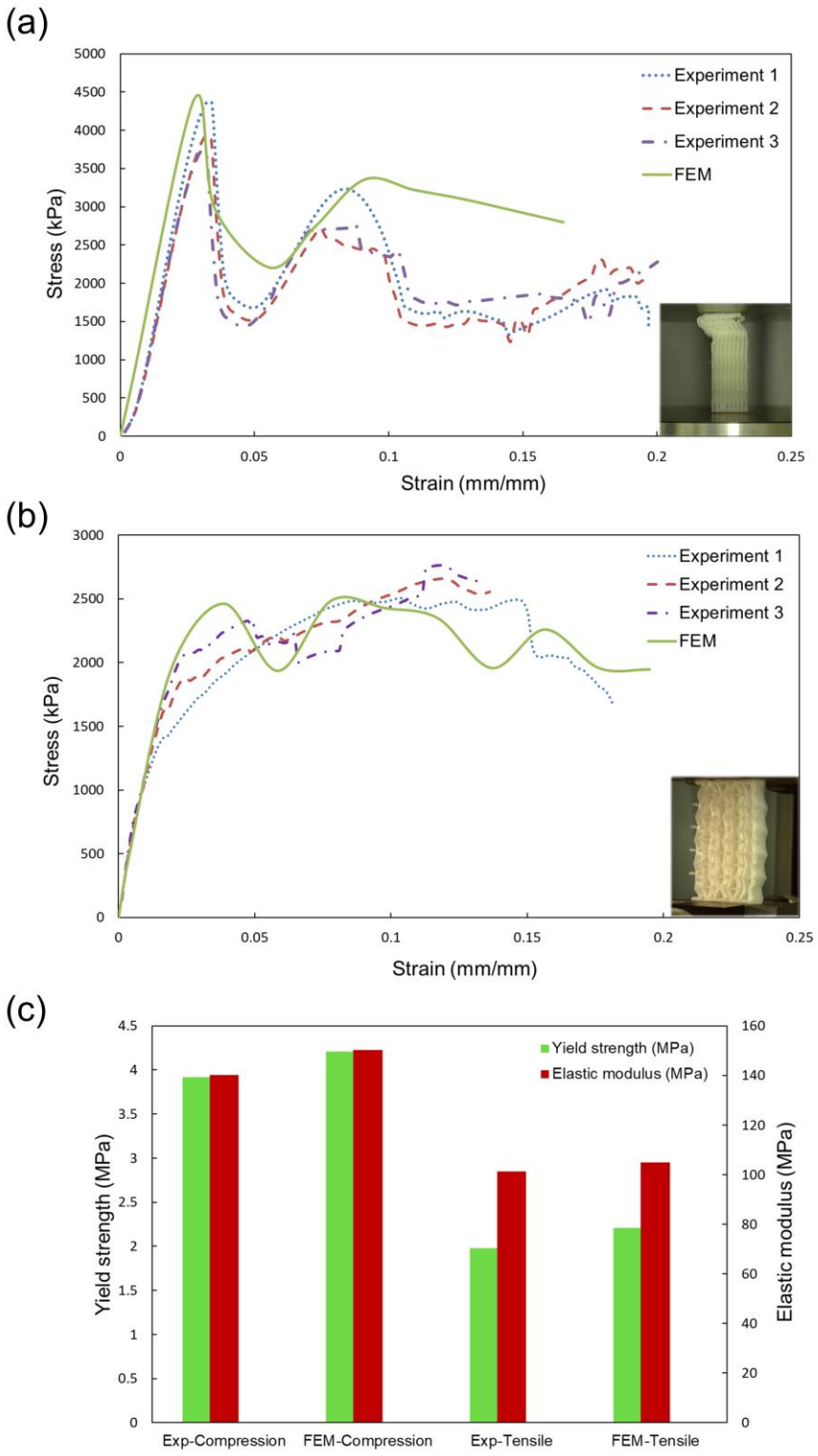

Figure 5. Mechanical properties of the conventional auxetic structure. Stress-strain curves of (a) compression and (b) tensile tests. (c) Elastic modulus and yield strength of the experimental tests (Exp) and simulation (FEM).

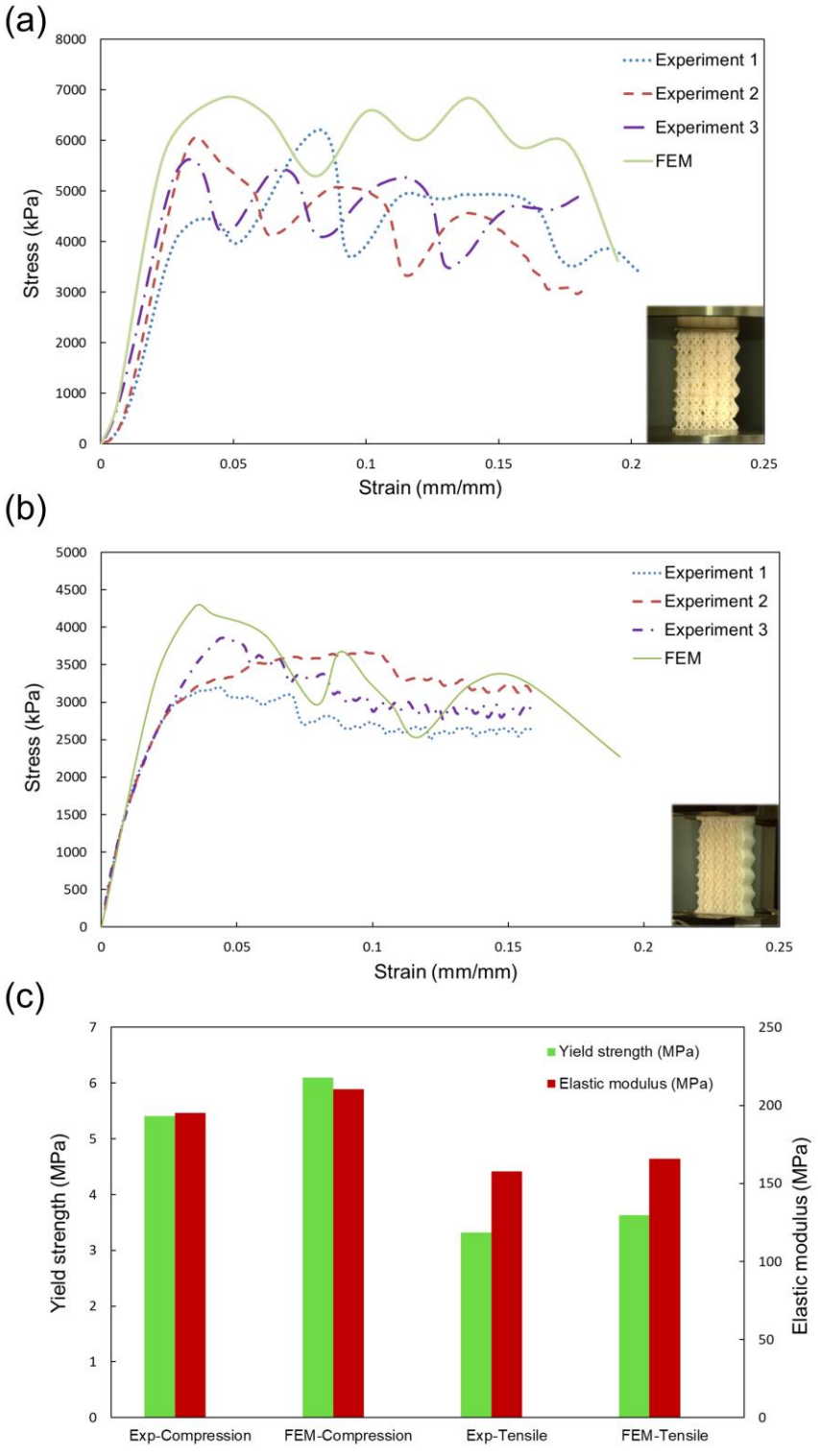

Figure 6. Mechanical properties of the triangle auxetic structure. Stress-strain curves of (a) compression and (b) tensile tests. (c) Elastic modulus and yield strength of the experimental tests (Exp) and simulation (FEM).

Table 2 presents the Poisson's ratio for both the conventional and triangle auxetic structures. The Poisson's ratio changes from -0.512 in the conventional auxetic structure to -0.225 in the triangle auxetic structure. However, both Young's modulus and yield strength increase under tensile and compression loads. The triangle auxetic structure exhibits a 28% increase in Young's modulus and a 27.5% increase in yield strength under compression, and a 35% increase in Young's modulus and a 40% increase in yield strength under tensile loading. The lower absolute value of the Poisson's ratio, which was achieved by triangle auxetic structure, is desirable for applications that require near zero Poisson's ratio and high mechanical properties, such as cancellous bone regeneration (Shirzad et al., 2022; Williams and Lewis, 1982). The normal range of Young's modulus for human cancellous bone is 10 MPa to 2 GPa, and the yield strength varies between 0.2 MPa to 80 MPa (Almela et al., 2017). The results demonstrate that the mechanical properties of the triangle auxetic structure fall within these ranges, and it can be an ideal choice for bone tissue engineering. The improved mechanical properties in the triangle auxetic structure are due to better stress distribution in comparison to the conventional auxetic structure. Figure 7 and 8 supports this assertion and shows the superiority of the triangle auxetic structures for both tensile and compression loads. Additionally, due to the lower elastic modulus of the conventional auxetic structure, it faces a critical buckling load (Figure 5a and Figure 7a). In contrast, the triangle auxetic structure does not show a local buckling pattern and can better distribute the loads. Under the tensile load, the inclined struts in conventional auxetic design should tolerate high tension and transverse deformation (Figures 8a and b). However, the transverse deformation and stress can be controlled by the novel design of the triangle auxetic structure (Figures 8 c and d).

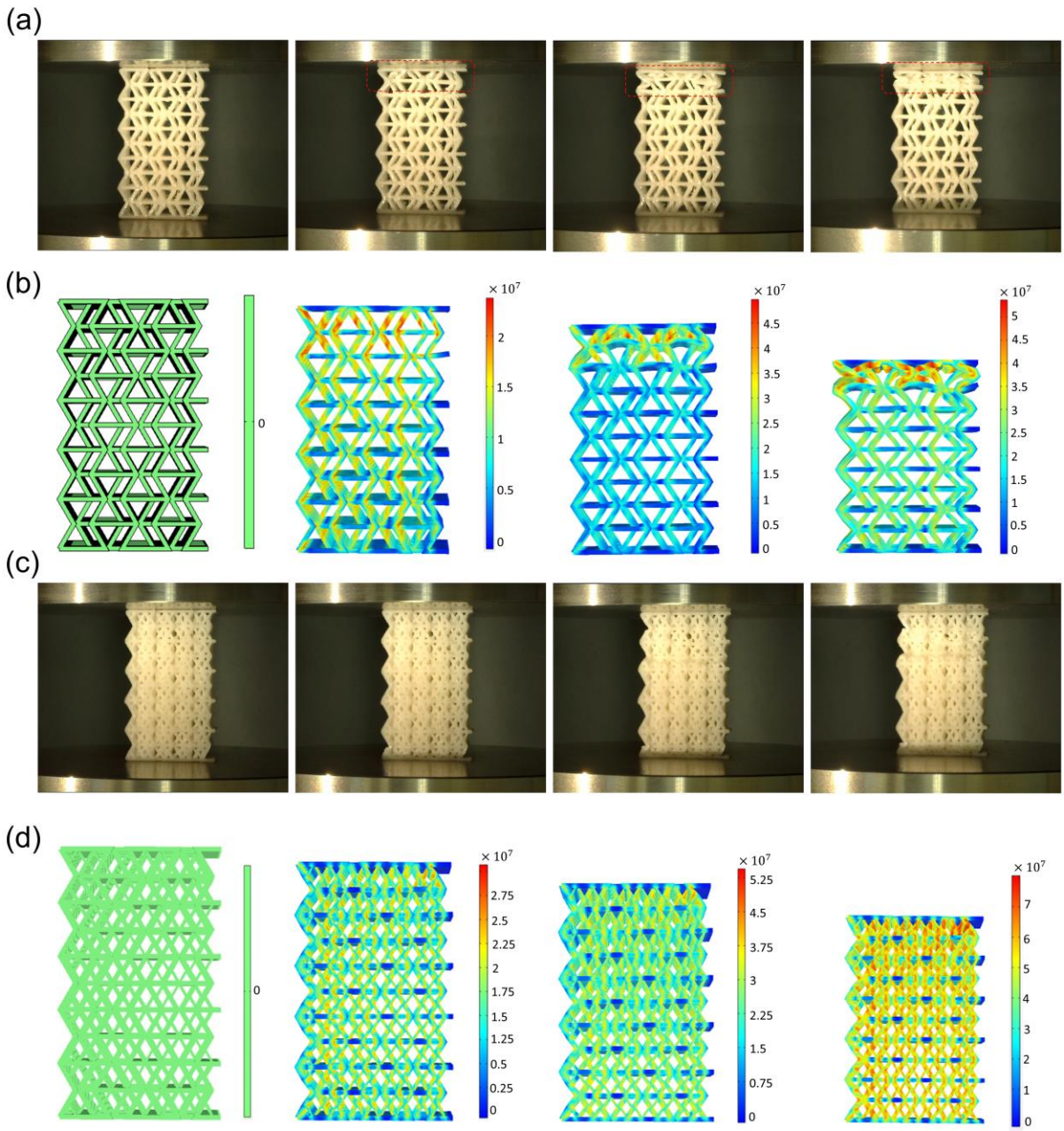

Figure 7. Deformation of conventional auxetic structure under compression load: (a) experimental results and (b) FE results (unit is Pa). Deformation of the tringle auxetic structure: (c) experimental results and (d) FE results (unit is Pa).

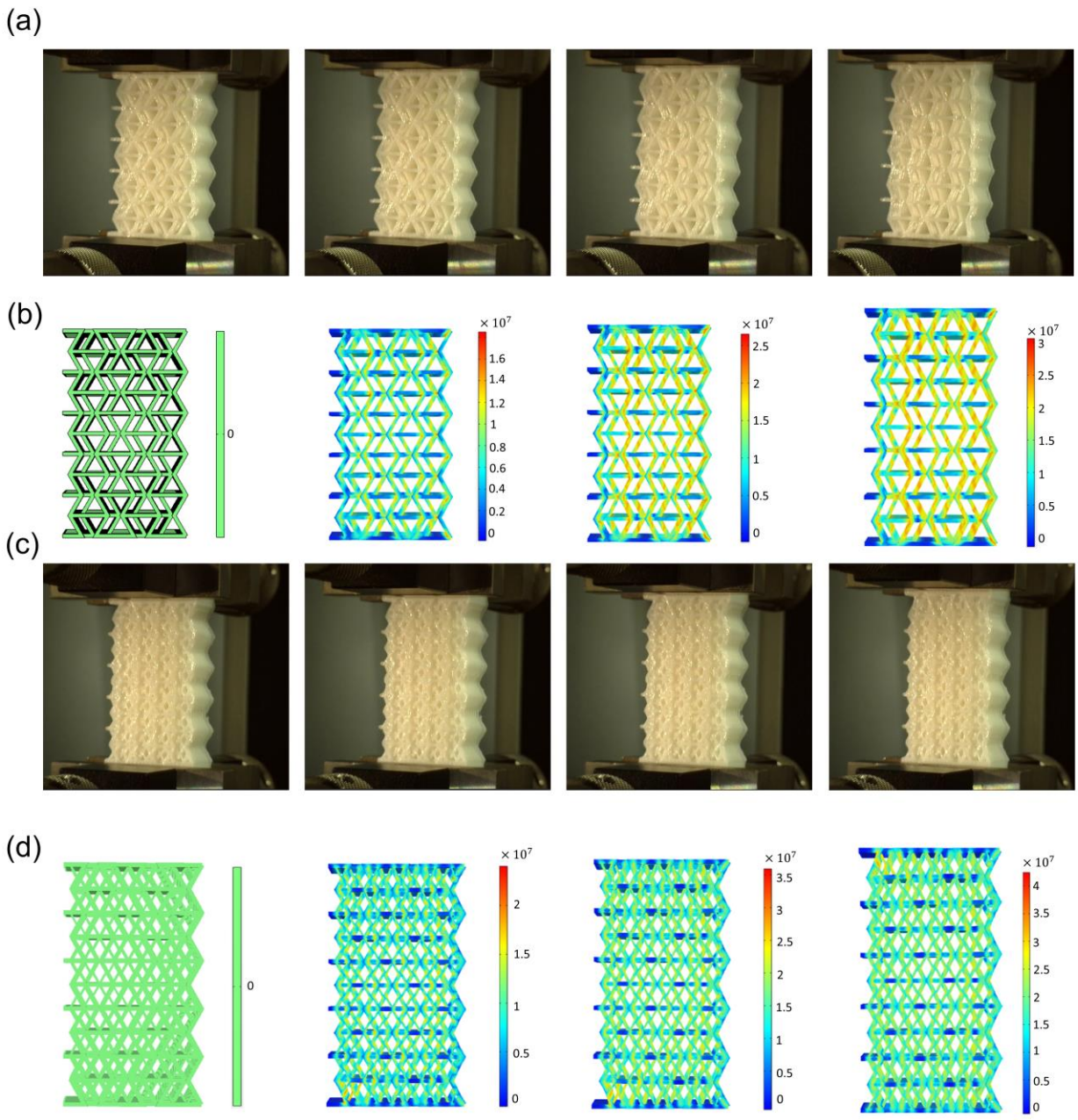

Figure 8. Deformation of conventional auxetic structure under tensile load: (a) experimental results and (b) FE results (unit is Pa). Deformation of the tringle auxetic structure: (c) experimental results and (d) FE results (unit is Pa).

Table 2. Poisson's ratio of conventional auxetic and triangle auxetic structure

Structure	Conventional auxetic		Triangle auxetic	
	Experimental	Numerical	Experimental	Numerical
Poisson's ratio	-0.512	-0.560	-0.225	-0.255

3.2. Optimization of mechanical properties of triangle auxetic gradient structure

Improving the mechanical properties of the scaffolds is crucial in bone tissue engineering to fabricate scaffolds with higher porosity and durability. Higher porosity allows for the appropriate diffusion of nutrients and oxygen to the defective organ, making it an essential feature for bone regeneration (Foroughi and Razavi, 2022; Jiao et al., 2022; Shirzad et al., 2021). Therefore, in this research, multi-objective optimization is performed to improve the mechanical properties of the triangle auxetic gradient structure. To mimic the structure of a real bone, scaffolds should possess identical gradient structures. Hence, in the first stage, a gradient structure with m = 8 mm and k = 5 mm is designed and evaluated by FEM (Table 3). The gradient triangle auxetic structure enhances the compression and tensile properties by 13% and 35% for Young's modulus and yield strength under compressive load, and 7% and 22% under tensile load, respectively. Notably, both the triangle and gradient triangle auxetic structures have almost the same porosities, which can be explained by the variable auxeticity of the gradient structure. Under the tensile or compression load, the first lower auxetic structure will be deformed; afterward, loads reach the higher auxetic structures. The higher auxeticity of the higher gradient layers can support the load-bearing behavior of the gradient triangle auxetic structures (Wanniarachchi et al., 2022). Furthermore, the lower porosity in the lower part of the gradient structure improves the load-bearing capacity and enhances Young's modulus and yield strength under various types of load (Wang et al., 2019).

The present study is not limited to a single case of improving the mechanical properties of the gradient triangle auxetic structure and aims to find the best architecture using FEM and experimental methods. The

proposed optimum architecture with high porosity is considered beside the compressive and tensile behavior of the gradient triangle auxetic structures. Consequently, gradient triangle structures with different physical variables are proposed to achieve higher mechanical properties with high porosity. The design variables of gradient triangle auxetic structures are presented in Table 3, where the ratio between m and k (m/k) is named as strut ratio.

Table 3. Physical and mechanical properties of the gradient triangle structures.

Size of struts	Strut ratio	Compressive elastic modulus (MPa)	Compressive yield strength (MPa)	Tensile elastic modulus (MPa)	Tensile yield strength (MPa)	Porosity (%)
m=7, k=4	1.75	366.88	6.96	228.44	4.38	64.4
m=7, k=4.5	1.55	350.92	6.41	260.21	4.77	67.1
m=7.5, k=4	1.87	371.37	7.51	240.41	5.01	67.3
m=7.5, k=4.5	1.66	248.08	5.16	206.13	4.14	68.2
m=7.5, k=5	1.5	288.07	5.36	193.14	3.52	70.1
m=8, k=4	2	237.67	4.85	147.55	3.01	67.6
m=8, k=4.5	1.77	355.77	6.88	231.18	4.38	68.9
m=8, k=5	1.6	226.33	8.43	170.92	4.26	70.5
m=8, k=5.5	1.45	323.45	5.55	208.41	2.97	71.1
m=8.5, k=4	2.125	343.17	7.66	183.21	4.06	68.1
m=8.5, k=4.5	1.88	375.65	7.59	227.81	4.53	70.2
m=8.5, k=5	1.7	338.55	6.41	172.48	3.28	71.2

m=8.5, k=5.5	1.54	359.29	6.41	218.81	3.58	72.8
m=8.5, k=6	1.41	267.41	4.38	187.43	2.97	73.4
m=9, k=4	2.25	286.82	6.33	181.64	4.3	69.3
m=9, k=4.5	2	384.28	8.13	264.06	5.61	70.6
m=9, k=5	1.8	370.87	6.73	195.73	3.52	71.8
m=9, k=5.5	1.63	276.33	4.85	220.93	3.75	73.3
m=9, k=6	1.5	370.33	6.02	251.61	3.95	74.3

Porosity is a critical factor in the design of bone scaffolds as appropriately interconnected pores permit tissue growth and nutrient diffusion. Cancellous bone typically requires 70-80% porosity to support nutrient diffusion (Fabbri et al., 2010; Liang et al., 2022; Seyednejad et al., 2011). The porosities of the gradient architectures are provided in Figure 9, and the gradient structures with porosities higher than 70% are chosen for the high porosity requirement for bone tissue engineering. The next step is to evaluate the mechanical properties of the gradient structures to find those with higher Young's modulus and yield strength while maintaining porosities of 70% or higher. When m = 7 or 7.5 mm, lower values of k are more reliable due to the controlling deformation of the inclined struts by the triangle parts. However, this phenomenon does not follow for higher values f m. The mechanical properties of gradient structures do not linearly increase or decrease with changing the size of inclined struts. This non-linear behavior has been confirmed by analytical studies using auxetic structures (Shen et al., 2021; Yang et al., 2015). Except for Figure 10 (b), in all cases, m = 9 mm and k = 4.5 mm exhibit higher mechanical properties under tensile and compression loads (Figure 10 (a), (c), and (d)). Therefore, this gradient triangle auxetic structure is selected for fabrication, evaluation, and experimental verification. The accuracy of the FEM prediction is confirmed in Figure 11. The suggested approach offers a low-cost method for identifying the optimum mechanical and high porosity gradient auxetic scaffold for bone tissue engineering.

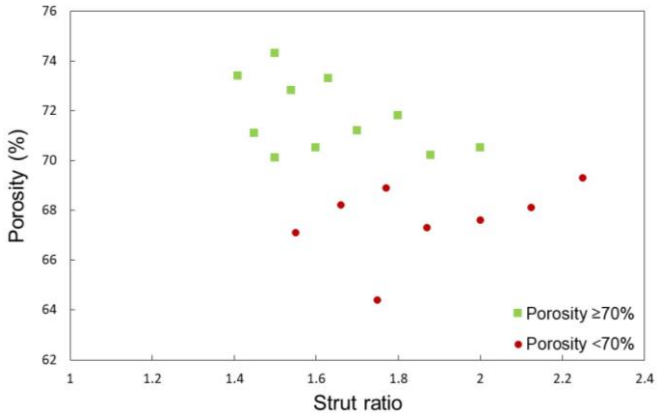

Figure 9. Porosity of different gradient triangle auxetic structures.

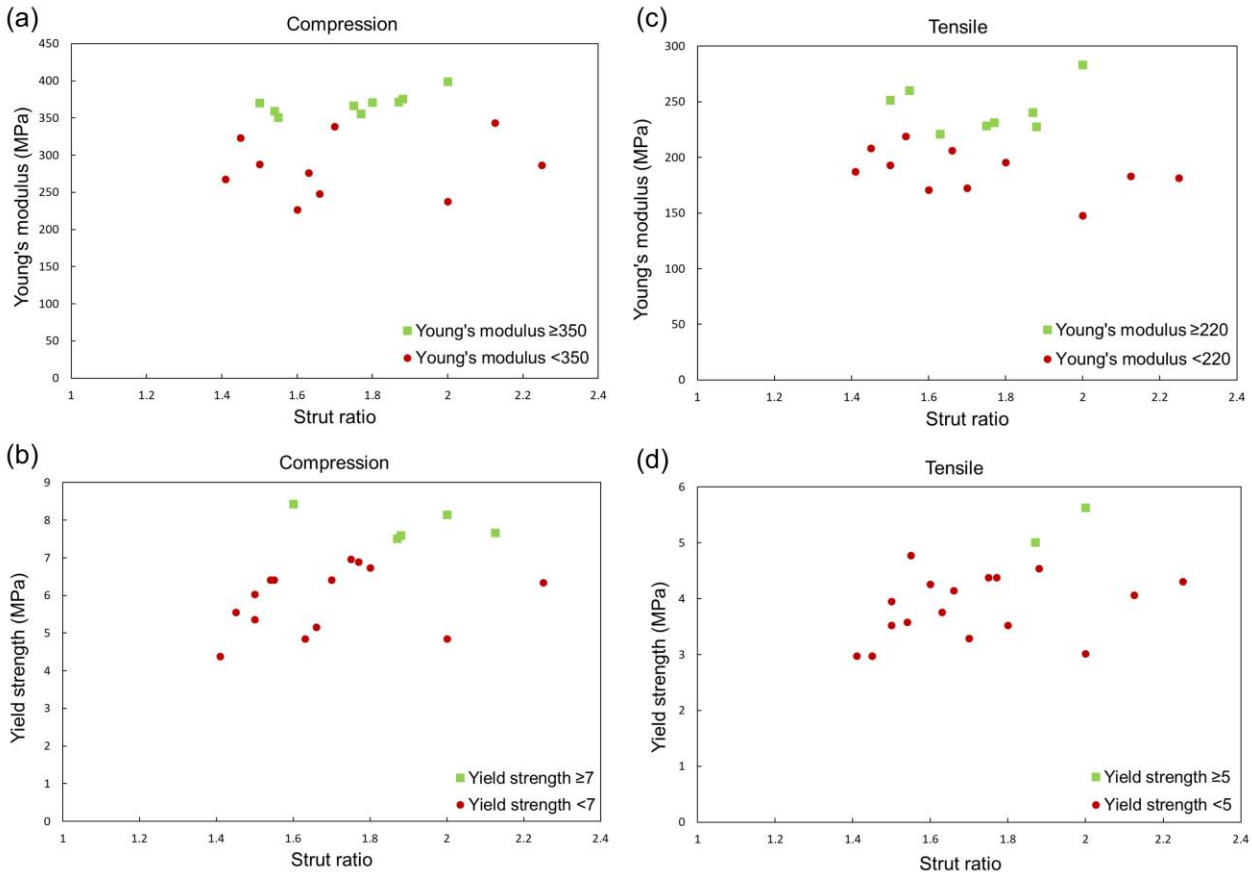

Figure 10. Mechanical properties of gradient triangle auxetic structures with optimum points (green points). Compression: (a) Young's modulus and (b) yield strength. Tensile: (c) Young's modulus and (d) yield strength.

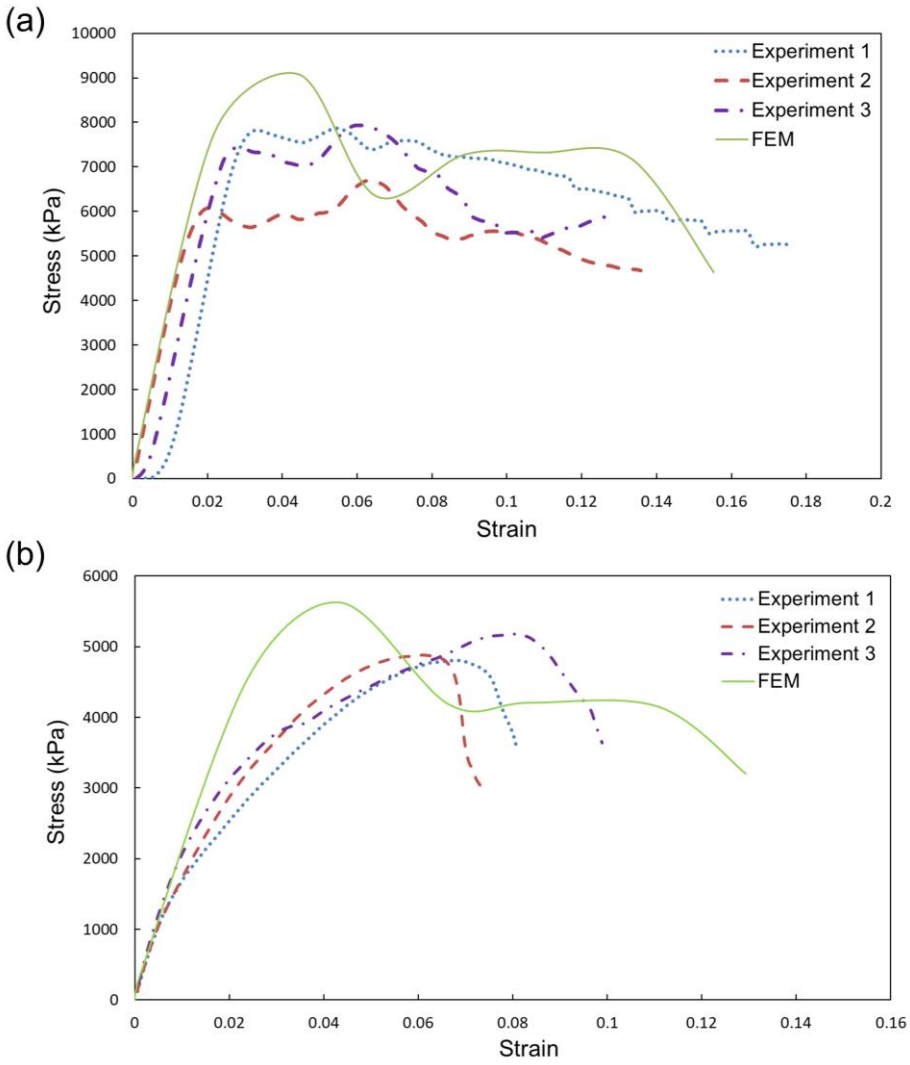

Figure 11. Experimental and numerical results of optimum gradient triangle auxetic structure. Stress-strain curves of (a) compression and (b) tensile tests.

Tendons serve as connective tissues that transmit forces from muscles to bones. The crimped structure of tendons grants them NPR behavior under load, making them highly tolerant of deformation and able to withstand high loads (Ruiz-Alonso et al., 2021). Thus, it is essential to design scaffolds with NPR characteristics and a high capacity to bear tensile loads. Furthermore, the hierarchical structure of tendons should be considered during scaffold design to replicate their natural properties (Zhang et al., 2022b). The triangle gradient structure with optimal parameters can serve as an effective tendon scaffold because of its gradient design, ability to tolerate high tensile loads, and NPR behavior. Nevertheless, several challenges must be addressed in this field. For instance, human tendons possess high negative Poisson's ratios, such

as the Achilles tendon's ratio of -1.44, requiring super-soft material with high deformation tolerance and load bearing capacity (Gatt et al., 2015). Reducing the size of unit cells is another challenge, requiring high resolution and accuracy of printing. This challenge can be overcome using stereolithography or high-accuracy bioprinting technology. Moreover, the high mechanical properties including Young's modulus of the bone-to-tendon around 800 MPa and its yield strength equal to approximately 70 MPa present a final challenge (Wren et al., 2001). Future work could explore the fabrication of scaffolds with high NPR structures with those mechanical properties.

4. Conclusion

In this study, a novel bioinspired auxetic structure for use in tendon and bone scaffolds was proposed, and compared its mechanical properties to those of a conventional auxetic structure. The results showed a 4% increase in porosity and significant improvements in mechanical properties with the triangle auxetic structure, making it an ideal choice for further investigation. Additionally, a gradient architecture was developed to mimic real bone and tendon tissues and investigated using FEM as well as experimental compression and tensile tests. The identical gradient triangle auxetic structure demonstrated a 13% increase in compressive Young's modulus and a 35% increase in compressive yield strength compared to the normal triangle auxetic structure, with a similar increase observed as 7% and 22% increases under tensile loads, respectively. By studying different physical conditions while maintaining high porosity and mechanical properties, the gradient structure was further improved. These results support the claim that the present novel gradient structure has the potential to be used in bone tissue engineering and other auxetic tissues in the human body such as tendons. The experimental and FEM results presented in this study provide a foundation for future research and development of bioinspired auxetic structures for tissue engineering applications.

Acknowledgment

This research was supported by a National Research Foundation of Korea (NRF) grant (NRF-2021R1I1A3040459) funded by the Korean government (MOE). This research was supported by a grant

of the Korea Health Technology R&D Project through the Korea Health Industry Development Institute (KHIDI), funded by the Ministry of Health & Welfare, Republic of Korea (grant number: HI22C1323).

References

Abifarin, J.K., Prakash, C., Singh, S., 2022. Optimization and significance of fabrication parameters on the mechanical properties of 3D printed chitosan/PLA scaffold. Materials Today: Proceedings 50, 2018-2025.
Ahmed, N., 2019. Direct metal fabrication in rapid prototyping: A review. Journal of Manufacturing Processes 42, 167-191.
Alizadeh-Osgouei, M., Li, Y., Vahid, A., Ataee, A., Wen, C., 2021. High strength porous PLA gyroid scaffolds manufactured via fused deposition modeling for tissue-engineering applications. Smart Materials in Medicine 2, 15-25.
Almela, T., Brook, I.M., Khoshroo, K., Rasoulianboroujeni, M., Fahimipour, F., Tahriri, M., Dashtimoghadam, E., El-Awa, A., Tayebi, L., Moharamzadeh, K., 2017. Simulation of cortico-cancellous bone structure by 3D printing of bilayer calcium phosphate-based scaffolds. Bioprinting 6, 1-7.
Fabbri, P., Bondioli, F., Messori, M., Bartoli, C., Dinucci, D., Chiellini, F., 2010. Porous scaffolds of polycaprolactone reinforced with in situ generated hydroxyapatite for bone tissue engineering. Journal of Materials Science: Materials in Medicine 21, 343-351.
Flamourakis, G., Spanos, I., Vangelatos, Z., Manganas, P., Papadimitriou, L., Grigoropoulos, C., Ranella, A., Farsari, M., 2020. Laser-made 3D auxetic metamaterial scaffolds for tissue engineering applications. Macromolecular Materials and Engineering 305, 2000238.
Foroughi, A.H., Razavi, M.J., 2022. Multi-objective Shape Optimization of Bone Scaffolds: Enhancement of Mechanical Properties and Permeability. Acta Biomaterialia.
Francisco, M.B., Pereira, J.L.J., Oliver, G.A., Roque da Silva, L.R., Cunha Jr, S.S., Gomes, G.F., 2021. A review on the energy absorption response and structural applications of auxetic structures. Mechanics of Advanced Materials and Structures, 1-20.
Gatt, R., Wood, M.V., Gatt, A., Zarb, F., Formosa, C., Azzopardi, K.M., Casha, A., Agius, T.P., Schembri-Wismayer, P., Attard, L., 2015. Negative Poisson's ratios in tendons: an unexpected mechanical response. Acta biomaterialia 24, 201-208.
Ghazlan, A., Nguyen, T., Ngo, T., Linforth, S., 2020. Performance of a 3D printed cellular structure inspired by bone. Thin-Walled Structures 151, 106713.
Guo, W., Jiang, Z., Zhong, H., Chen, G., Yan, H., Zhang, C., Zhao, L., 2023. 3D printing of multifunctional gradient bone scaffolds with programmable component distribution and hierarchical pore structure. Composites Part A: Applied Science and Manufacturing 166, 107361.
Jiao, C., Xie, D., He, Z., Liang, H., Shen, L., Yang, Y., Tian, Z., Wu, G., Wang, C., 2022. Additive manufacturing of Bio-inspired ceramic bone Scaffolds: Structural Design, mechanical properties and biocompatibility. Materials & Design 217, 110610.
Kim, K., Dean, D., Wallace, J., Breithaupt, R., Mikos, A.G., Fisher, J.P., 2011. The influence of stereolithographic scaffold architecture and composition on osteogenic signal expression with rat bone marrow stromal cells. Biomaterials 32, 3750-3763.
Kim, M.J., Choi, H.J., Cho, J., Lee, J.B., Sung, H.-J., Kim, J.K., 2017. MG-63 Cell Proliferation with Static or Dynamic Compressive Stimulation on an Auxetic PLGA Scaffold. International Journal of Polymer Science 2017.
Kim, W., Kim, M., Kim, G.H., 2018. 3D-printed biomimetic scaffold simulating microfibril muscle structure. Advanced Functional Materials 28, 1800405.
Kolken, H., Garcia, A.F., Du Plessis, A., Meynen, A., Rans, C., Scheys, L., Mirzaali, M., Zadpoor, A., 2022. Mechanisms of fatigue crack initiation and propagation in auxetic meta-biomaterials. Acta Biomaterialia 138, 398-409.
Liang, H., Wang, Y., Chen, S., Liu, Y., Liu, Z., Bai, J., 2022. Nano-Hydroxyapatite Bone Scaffolds with Different Porous Structures Processed by Digital Light Processing 3D Printing. International Journal of Bioprinting 8.
Lira, C., Scarpa, F., Rajasekaran, R., 2011. A gradient cellular core for aeroengine fan blades based on auxetic configurations. Journal of Intelligent Material Systems and Structures 22, 907-917.
Liu, F., Zhang, D.Z., Zhang, P., Zhao, M., Jafar, S., 2018. Mechanical properties of optimized diamond lattice structure for bone scaffolds fabricated via selective laser melting. Materials 11, 374.

Lvov, V.A., Senatov, F.S., Veveris, A.A., Skrybykina, V.A., Díaz Lantada, A., 2022. Auxetic Metamaterials for Biomedical Devices: Current Situation, Main Challenges, and Research Trends. Materials 15, 1439.
Nuge, T., Tshai, K.Y., Lim, S.S., Nordin, N., Hoque, M.E., 2020. Characterization and optimization of the mechanical properties of electrospun gelatin nanofibrous scaffolds. World Journal of Engineering.
Peng, B., Li, J., Wu, J., Chen, N., Chen, G., 2022. Preparation and performance of poly (vinyl alcohol)/polylactic acid/hydroxyapatite composite scaffolds based on 3D printing. Journal of Applied Polymer Science 139, 51534.
Ruhela, A., Bhatt, A., Rath, S.N., Sharma, C.S., 2023. Biomimicking tendon by electrospinning tissue-derived decellularized extracellular matrix for tendon tissue engineering. Journal of Applied Polymer Science, e53368.
Ruiz-Alonso, S., Lafuente-Merchan, M., Ciriza, J., Saenz-del-Burgo, L., Pedraz, J.L., 2021. Tendon tissue engineering: Cells, growth factors, scaffolds and production techniques. Journal of Controlled Release 333, 448-486.
Sahariah, B.J., Namdeo, A., Khanikar, P., 2022. Composite-inspired multilattice metamaterial structure: An auxetic lattice design with improved strength and energy absorption. Materials Today Communications 30, 103159.
Sala, R., Regondi, S., Pugliese, R., 2022. Design Data and Finite Element Analysis of 3D Printed Poly (ε-Caprolactone)-Based Lattice Scaffolds: Influence of Type of Unit Cell, Porosity, and Nozzle Diameter on the Mechanical Behavior. Eng 3, 9-23.
Sankineni, R., Ravi Kumar, Y., 2022. Evaluation of energy absorption capabilities and mechanical properties in FDM printed PLA TPMS structures. Proceedings of the Institution of Mechanical Engineers, Part C: Journal of Mechanical Engineering Science 236, 3558-3577.
Seyednejad, H., Gawlitta, D., Dhert, W.J., Van Nostrum, C.F., Vermonden, T., Hennink, W.E., 2011. Preparation and characterization of a three-dimensional printed scaffold based on a functionalized polyester for bone tissue engineering applications. Acta biomaterialia 7, 1999-2006.
Shen, J., Liu, K., Zeng, Q., Ge, J., Dong, Z., Liang, J., 2021. Design and mechanical property studies of 3D re-entrant lattice auxetic structure. Aerospace Science and Technology 118, 106998.
Shirzad, M., Fathi, A., Rabiee, S.M., Ghaffari, S., Zabihi-Neishabouri, E., 2020. Three-dimensional printing of truss-like structure for use in scaffold: Experimental, numerical, and analytical analyses. Proceedings of the Institution of Mechanical Engineers, Part C: Journal of Mechanical Engineering Science 234, 3133-3142.
Shirzad, M., Zolfagharian, A., Bodaghi, M., Nam, S.Y., 2022. Auxetic metamaterials for bone-implanted medical devices: Recent advances and new perspectives. European Journal of Mechanics-A/Solids, 104905.
Shirzad, M., Zolfagharian, A., Matbouei, A., Bodaghi, M., 2021. Design, evaluation, and optimization of 3D printed truss scaffolds for bone tissue engineering. Journal of the mechanical behavior of biomedical materials 120, 104594.
Solomon, I.J., Sevvel, P., Gunasekaran, J., 2021. A review on the various processing parameters in FDM. Materials Today: Proceedings 37, 509-514.
Soman, P., Lee, J.W., Phadke, A., Varghese, S., Chen, S., 2012. Spatial tuning of negative and positive Poisson's ratio in a multi-layer scaffold. Acta biomaterialia 8, 2587-2594.
Tanodekaew, S., Channasanon, S., Kaewkong, P., Uppanan, P., 2013. PLA-HA scaffolds: preparation and bioactivity. Procedia Engineering 59, 144-149.
Tortorici, M., Gayer, C., Torchio, A., Cho, S., Schleifenbaum, J.H., Petersen, A., 2021. Inner strut morphology is the key parameter in producing highly porous and mechanically stable poly (ε-caprolactone) scaffolds via selective laser sintering. Materials Science and Engineering: C 123, 111986.
Wang, C., Vangelatos, Z., Grigoropoulos, C.P., Ma, Z., 2022a. Micro-engineered architected metamaterials for cell and tissue engineering. Materials Today Advances 13, 100206.
Wang, M., Wu, H., Yang, L., Chen, A., Chen, P., Wang, H., Chen, Z., Yan, C., 2022b. Structure design of arc-shaped auxetic metamaterials with tunable Poisson's ratio. Mechanics of Advanced Materials and Structures, 1-11.
Wang, X., Zhao, L., Fuh, J.Y.H., Lee, H.P., 2019. Effect of porosity on mechanical properties of 3D printed polymers: Experiments and micromechanical modeling based on X-ray computed tomography analysis. Polymers 11, 1154.
Wanniarachchi, C.T., Arjunan, A., Baroutaji, A., Singh, M., 2022. Mechanical performance of additively manufactured cobalt-chromium-molybdenum auxetic meta-biomaterial bone scaffolds. journal of the mechanical behavior of biomedical materials 134, 105409.
Warner, J.J., Gillies, A.R., Hwang, H.H., Zhang, H., Lieber, R.L., Chen, S., 2017. 3D-printed biomaterials with regional auxetic properties. Journal of the mechanical behavior of biomedical materials 76, 145-152.
Williams, J., Lewis, J., 1982. Properties and an anisotropic model of cancellous bone from the proximal tibial epiphysis.
Wren, T.A., Yerby, S.A., Beaupré, G.S., Carter, D.R., 2001. Mechanical properties of the human achilles tendon. Clinical biomechanics 16, 245-251.
Yang, L., Harrysson, O., West, H., Cormier, D., 2015. Mechanical properties of 3D re-entrant honeycomb auxetic structures realized via additive manufacturing. International Journal of Solids and Structures 69, 475-490.

Yang, Z., Niksiar, P., Meng, Z., 2022. Identifying structure-property relationships of micro-architectured porous scaffolds through 3D printing and finite element analysis. Computational Materials Science 202, 110987.
Zhang, J., Chen, X., Sun, Y., Yang, J., Chen, R., Xiong, Y., Hou, W., Bai, L., 2022a. Design of a biomimetic graded TPMS scaffold with quantitatively adjustable pore size. Materials & Design 218, 110665.
Zhang, S., Ju, W., Chen, X., Zhao, Y., Feng, L., Yin, Z., Chen, X., 2022b. Hierarchical ultrastructure: An overview of what is known about tendons and future perspective for tendon engineering. Bioactive Materials 8, 124-139.
Zhang, T., Li, S., Chen, Y., Xiao, H., Wang, L., Hu, J., Xu, D., Lu, H., 2022c. Characterize the microstructure change after tendon enthesis injury using synchrotron radiation μCT. Journal of Orthopaedic Research®.